Control of an helicopter main gearbox active suspension system

Jonathan Rodriguez, Luc Gaudiller, Simon Chesné, Paul Cranga

CONTROL OF A HELICOPTER MAIN GEARBOX ACTIVE SUSPENSION SYSTEM

Jonathan RODRIGUEZ
Airbus Helicopters - Dynamics and Vibrations
Marignane, France
LAMCOS - INSA - Lyon,France
jonathan.rodriguez@airbus.com

Luc GAUDILLER
Simon CHESNE
LAMCOS INSA - Lyon, France
Structure Dynamics Department
luc.gaudiller@insa-lyon.fr
simon.chesne@insa-lyon.fr

Paul Cranga
Airbus Helicopters - Dynamics and Vibrations
Marignane, France
paul.cranga@airbus.com

ABSTRACT

This paper considers the control of a helicopter gearbox electromagnetic suspension for a complete multibody model of the structure. As the new generation of helicopters includes variable engine RPM during flight, it becomes relevant to add active control in their suspension systems. Most of active system performances derive directly from the controller construction, its optimization to the system controlled and the disturbances expected. An investigation on a FXLMS control algorithm has been made to optimize it in terms of narrow band disturbance rejection. In this paper an active suspension based on DAVI principle is evaluated. Firstly, a multibody model is set up to estimate realistic acceleration levels inside the cabin. Then multiple controllers are tested, minimizing vibrations on different parts of the helicopter structure. The simulations tend to prove that it is possible to implement an effective active suspension with a low power actuator and obtain a significant vibration reduction level for a frequency bandwidth centered at the natural frequency of the original DAVI.

NOMENCLATURE

b Number of blades of the main rotor
Ω Rotational speed of the main rotor $[rad.s^{-1}]$
MGB Main gearbox
FR front right actuator
FL front left actuator
RR rear right actuator
RL rear left actuator
V Potential energy
T Kinetic energy
$\underline{Q^{nc}}$ Non conservative generalized forces
$\underline{q}$ Generalized coordinates vector
$\underline{\tau}$ Actuation vector
$\underline{M}$ Mass matrix
$\underline{K}$ Stiffness matrix
$\underline{D}$ Damping matrix
ξ_i modal damping of the i^{th} mode
K_f voice coil actuator force constant
K_s voice coil actuator back EMF constant
R voice coil actuator resistance
L_a voice coil actuator inductivity
x_{act} voice coil actuator displacement
Φ modes shape matrix
F_{x_i} dynamic force magnitude on longitudinal axis for i^{th} harmonic
F_{y_i} dynamic force magnitude on lateral axis for i^{th} harmonic
F_{z_i} dynamic force magnitude on vertical axis for i^{th} harmonic
M_{x_i} dynamic moment magnitude on longitudinal axis for i^{th} harmonic
M_{y_i} dynamic moment magnitude norm on lateral axis for i^{th} harmonic
M_{z_i} dynamic moment magnitude norm on vertical axis for i^{th} harmonic
ϕ_{fx_i} dynamic force phase on longitudinal axis for i^{th} harmonic
ϕ_{fy_i} dynamic force phase on lateral axis for i^{th} harmonic

ϕ_{fz_i} dynamic force phase on vertical axis for i^{th} harmonic
ϕ_{mx_i} dynamic moment phase on longitudinal axis for i^{th} harmonic
ϕ_{my_i} dynamic moment phase on lateral axis for i^{th} harmonic
ϕ_{mz_i} dynamic moment phase on vertical axis for i^{th} harmonic
E number of error sensors
R number of actuators
L filtering order
$\mathbf{w}(t)$ weighting factors vector
$\mathbf{y}(t)$, $u(t)$ control command signals
$\mathbf{d}(t)$ disturbance signal vector
$\mathbf{e}(t)$ error signal vector
$\mathbf{x}(t)$ reference signal vector
$\mathbf{X}(t)$ reference signal matrix
$\mathbf{X}'(t)$ filtered reference signal matrix
$\hat{S}(s)$ transfer functions estimation matrix
μ convergence factor
α leak coefficient
Q weighting matrix for FXLMS
$[A\ B\ C\ D]$ state space system matrices

1 INTRODUCTION

Vibrations have always been a main issue in helicopter design, flight handling and crew comfort. Firstly, aerodynamic forces acting on blades create heavy cyclic loads on the rotor hub. Then, a helicopter includes many rotating parts at a wide range of frequencies from the engines to the main gearbox and the rotor hub. Finally, external aerodynamic charges coming from air flow exciting the structure also create vibrations inside the cabin. This paper will focus on the cyclic loads due to main rotor which major part of there energy is acting at the frequency $b\Omega$ (see [1] p290 to 294). Many passive anti-vibration devices were designed since the early 70's going from simple elastomeric mounts for the main gearbox to more complex vibration absorbers.

In 1976, Flannelly describes in [2] an anti-resonant vibration absorber called DAVI which uses a rigid arm carrying a small mass (bobweight mass). This flapping inertia creates an anti-resonance at the desired frequency depending on the tuning parameters (flapping mass, dynamic amplification, overall stiffness). Based on this principle, in the early 90's Eurocopter company develops the SARIB®, an efficient passive suspension between the main gear box and the structure creating an anti-resonance at the $b\Omega$ frequency. Another example of effective passive anti-resonant absorber is the Lord Fluidlastic® [3] which also applies the DAVI principle. A high density fluid with low viscosity (mercury was used for the first prototypes) is moving between two chambers. These two chambers communicate by an inner cylinder with a reduced section which create a dynamic amplification. The fluid inertia acts exactly the same as the tuning weight on the arm of the DAVI. Elastomeric parts play as mechanical spring and the overall system has a frequency response equivalent to the DAVI. Using a fluid allows a much more compact device but force to deal with its inherited viscosity, creating damping a the anti-resonance frequency and so lowering its efficiency.

With the fade-in of variable engine RPM during flight, it became relevant to consider having active suspension systems to "track" the main frequency $b\Omega$. Intents have been done to integrate such systems to the struts [4] but low power actuators could only control high frequency vibrations. In 1993, Eurocopter also developed in partnership with Liebherr an active hydraulic strut, able to counteract directly the low frequency rotor hub loads (see [1] for principle). The control was acting at 30Hz, 4 actuators were generating 2.5kN each and a 70% global vibration level reduction was achieved. Unfortunately the overall system remained too heavy and complex to maintain for an industrial application.

During the last years, active vibration absorbers have also been placed directly in the cabin to be as close as posible to the deck. In [5] and [6] it is shown that several low power actuators (1kW for the overall system) cleverly placed in the cabin, near structural parts could achieve a significant reduction in vibration level and adapt itselves to variable RPM with a suitable control. In 2006, Lord presented its well known Fluidlastic® pylon in its active version [7]. An hydraulic actuator acts on the fluid and allows to control the output force of the pylon. Theoretically, the force generated by the actuator cancels the system damping due to the fluid at the anti-resonance frequency. The passive fluid inertia forces cancel around 70% of the input while the active force can virtually cancel the remaining 30%. The main advantage of DAVI principle combined with an active part is that the power required to cancel the $b\Omega$ frequency is much less than an active strut thanks to the anti-resonance phenomenon.

This paper considers control of a helicopter suspension between the main gearbox and the structure based on DAVI principle (Eurocopter SARIB®). Different FXLMS controllers will be compared. Efficiency will be studied for a bandwidth centered at the original anti-resonance frequency of the DAVI ($b\Omega + / - 10\%$). As for every controller, efficiency and power consumption will also be comparison criteria. Design of the controllers was done using a complete three-dimensionnal multibody model of the SARIB® suspension coupled to a rigid gear box and rotor hub and a modal base of a heavy-weight helicopter fuselage. The use of a full structure model allows to be more predictive about the vibration level expected in the cabin and have much more possibilitites of locations for the error sensors (force or acceleration).

The outline of the paper is as follows, in section 2 the system model will be discussed which consists of an introduction to the active SARIB® suspension, the fuselage model that will be used for simulation and the rotor dynamic loads. After this the main control problem will be presented and the controller design will

FIGURE 1: Airbus Helicopters NH90 helicopter

Variable	Description	Unit
m_f	Fuselage mass	$[kg]$
m_{mgb}	Main Gearbox mass	$[kg]$
m_{ba}	flapper arm	$[kg]$
m_{bm}	flapper mass	$[kg]$
m_e	engine mass	$[kg]$
m_r	rotor hub mass	$[kg]$
b	blade number	[-]
rotor speed	Ω	$[rad.s^{-1}]$

TABLE 1: NH90 main model parameters

be presented in detail. In section 5, the simulation results will be presented. Finally, conclusions are drawn in section 6.

2 SYSTEM MODEL

In this section will be described the model used for the simulation of the active suspension system. As a basis for the model set up, the Eurocopter NH90 was used (figure 1). First of all, it was one of the two Eurocopter helicopters to already have an operational passive SARIB® suspension. Then active suspensions are well suited for heavy-weight helicopters due to high level of vibrations coming from the rotor hub and the space available on the upper deck superior to smaller machines. In the table 1, the NH90 main parameters that are used for the multibody model are shown.

2.1 The active SARIB® suspension

The active SARIB® suspension based on DAVI principle (see figure 2) consists of 4 individual units around the gearbox. Each unit includes a leaf spring, a rigid flapper arm carrying the flapper mass and a strut to link the gearbox to it. A 2 dimensionnal view of the dynamic model of this system is presented on figure 3 and some main parameters are presented in the table 2. For more accurate behaviour of the model, it has been added

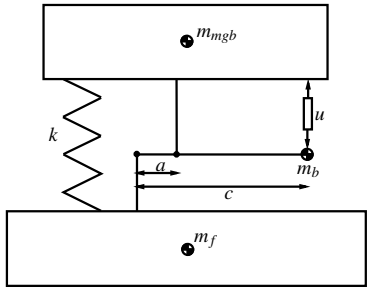

FIGURE 2: DAVI principle with active control

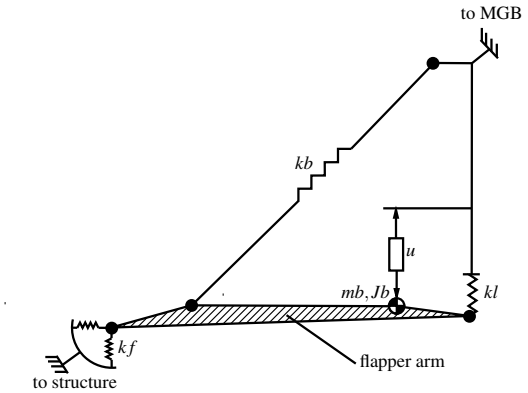

FIGURE 3: dynamic model of an isolated SARIB® unit

Variable	Description	Unit
m_b	flapper mass	$[kg]$
$J_{b,22}$	flapper inertia	$[kg.m^2]$
k_b	strut stiffness	$[N.m^{-1}]$
k_l	leaf spring stiffness	$[N.m^{-1}]$
k_f	fitting stiffness	$[N.m^{-1}]$

TABLE 2: SARIB® isolated unit main parameters

the struts stiffness (k_b), the fittings linking the flapper arm to the structure (k_f), and the leaf spring linking the flapper arm to the main gearbox (k_l). The command force u is generated by an actuator acting between the flapper mass and the main gearbox in order to control the relative rotational movement of the flapper arm with respect to the structure. As the inertia of the mass m_b defines the DAVI anti-resonance frequency, controlling its movement around this particular frequency allows a low power atuator like a voice-coil to significantly reduce the suspension's transmissibility for a small bandwidth.

Once the model of the isolated SARIB® unit is defined, it has to be implemented to a full three dimensional multibody model. As it is presented in figure 4, this model includes the ro-

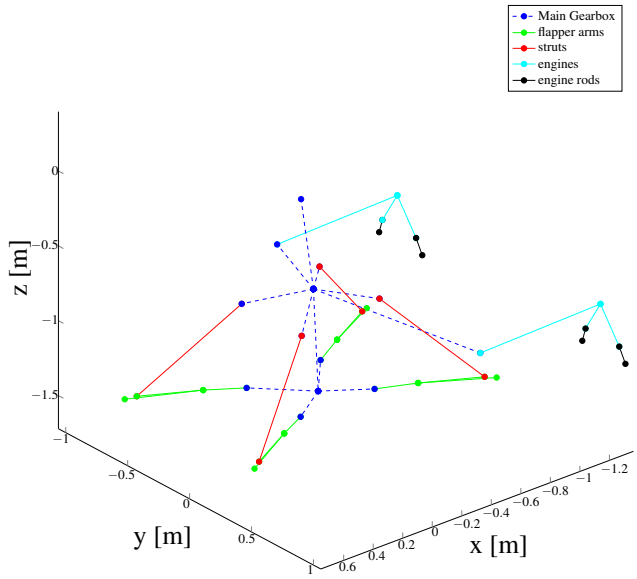

FIGURE 4: 3D SARIB suspension model

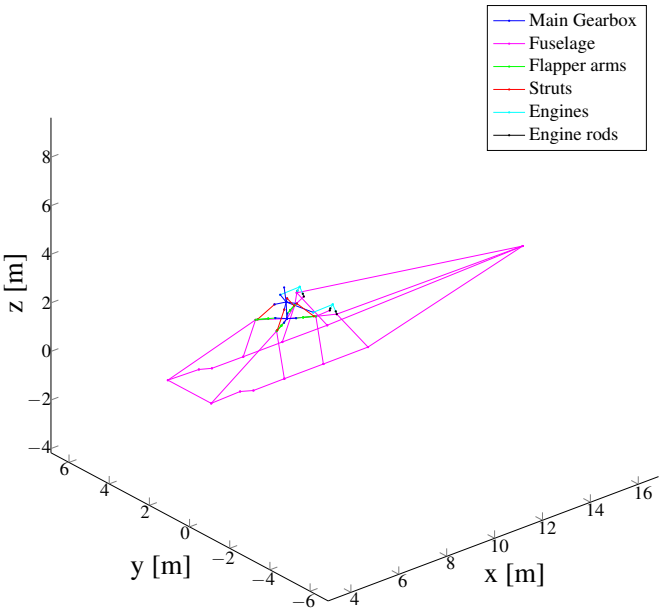

FIGURE 5: 3D SARIB suspension model with its associated helicopter structure

tor hub and the main gearbox linked rigidly, four SARIB® units, two engines with their links to the main gearbox and the structure. Equations of motion are first computed using Lagrangian method [8] as follows:

$$\frac{d}{dt}(T,_{\underline{\dot{q}}}) - T,_{\underline{q}} + V,_{\underline{q}} = (\underline{Q}^{nc})^T \tag{1}$$

As we avoid putting contraints in the system by replacing all joints between bodies by springs, Lagrange multipliers are not needed. The equation (1) can know be rewritten in the following form:

$$\underline{M}(\underline{q})\underline{\ddot{q}} + \underline{H}(\underline{q},\underline{\dot{q}}) = \underline{S}(\underline{q})\underline{\tau} \tag{2}$$

with the matrix $\underline{H}$ containing all Coriolis terms, joint flexibility effects and gravitationnal effects. In order to study the frequency behaviour of the model, we split the generalized coordinates $\underline{q} = \underline{q}_e + \underline{q}_l(t)$ in a constant part $\underline{q}_e$ corresponding to equilibrium point and a linear time dependent part $\underline{q}_l(t)$. This new formulation of (2) leads to the linearization of the problem and we obtain

$$\underline{M}\underline{\ddot{q}}_l(t) + \underline{D}\underline{\dot{q}}_l(t) + \underline{K}\underline{q}_l(t) = \underline{S}\ \underline{\tau}_l(t) \tag{3}$$

For frequency behaviour, it is more convenient to use modal damping. From the mass and stiffness matrices, the mode shapes matrix $\underline{\Phi}$ is computed by eigenvalue decomposition. The modal mass and modal stiffness are then defined as follows:

$$\begin{cases} \underline{M}_{mod} = \underline{\Phi}^T\ \underline{M}\ \underline{\Phi} \\ \underline{K}_{mod} = \underline{\Phi}^T\ \underline{K}\ \underline{\Phi} \end{cases} \tag{4}$$

With ξ_i as the modal damping coefficient of the i^{th} mode, The modal damping matrix $\underline{D}_{mod}$ is a diagonal matrix whose terms are

$$\underline{D}_{mod\ i} = 2\xi_i \sqrt{\underline{K}_{mod\ i}\ \underline{M}_{mod\ i}} \tag{5}$$

Finally, the matrix damping used is

$$\underline{D} = (\underline{\Phi}^T)^{-1} \underline{D}_{mod} \underline{\Phi}^{-1} \tag{6}$$

2.2 Fuselage model

Once the multibody model of the whole suspension is set up, it is coupled to a modal base from a fuselage FEM model (see [9]) condensated using Craig and Bampton method [10]. This model includes nodes situated at the pilot and copilot seats and feet added to eight nodes uniformly placed on deck and a node corresponding to the tail rotor (see figure 5). Let us define p the fuselage number of DOF, n the number of common nodes from the two models and m the free DOF of the suspension multibody

model. The fuselage mass and stiffness matrix extracted from Craig and Bampton are in the form:

$$\underline{M}_{fus} = \begin{bmatrix} \underline{I}_p & \underline{M}_{fus_{1,2}} \\ \underline{M}^T_{fus_{1,2}} & \underline{M}_{fus_{2,2}} \end{bmatrix} \quad \underline{K}_{fus} = \begin{bmatrix} \underline{K}_{fus_{1,1}} & 0 \\ 0 & \underline{K}_{fus_{2,2}} \end{bmatrix} \tag{7}$$

With $\underline{M}_{fus_{2,2}} \in \Re^{[n\times n]}$, $\underline{K}_{fus_{1,1}} \in \Re^{[p\times p]}$ and $\underline{K}_{fus_{2,2}} \in \Re^{[n\times n]}$. $\underline{K}_{fus_{1,1}}$ is defined as diagonal matrix. The multibody model presented in the previous section can also be rearranged to this form:

$$\underline{M} = \begin{bmatrix} \underline{M}_{1,1} & 0 \\ 0 & \underline{M}_{2,2} \end{bmatrix} \quad \underline{K} = \begin{bmatrix} \underline{K}_{1,1} & \underline{K}_{1,2} \\ \underline{K}_{2,1} & \underline{K}_{2,2} \end{bmatrix} \tag{8}$$

With $\underline{M}_{1,1} \in \Re^{[n\times n]}$,$\underline{M}_{2,2} \in \Re^{[m\times m]}$,$\underline{K}_{1,1} \in \Re^{[n\times n]}$ and $\underline{K}_{2,2} \in \Re^{[m\times m]}$. It is now obvious that the equations of motion of the complete model can be written as follows:

$$\begin{bmatrix} \underline{I}_p & \underline{M}_{fus_{1,2}} & 0 \\ \underline{M}^T_{fus_{1,2}} & \underline{M}_{fus_{2,2}} + \underline{M}_{1,1} & 0 \\ 0 & 0 & \underline{M}_{2,2} \end{bmatrix} \ddot{\underline{q}} + \tag{9}$$

$$\begin{bmatrix} \underline{K}_{fus_{1,1}} & 0 & 0 \\ 0 & \underline{K}_{fus_{2,2}} + \underline{K}_{1,1} & \underline{K}_{1,2} \\ 0 & \underline{K}_{2,1} & \underline{K}_{2,2} \end{bmatrix} \underline{q} + \underline{D}\,\dot{\underline{q}} = \begin{bmatrix} 0 \\ \underline{S} \end{bmatrix} \underline{\tau} \tag{10}$$

$\underline{S} \in \Re^{[(m+n)\times k]}$ with k defined as the number of inputs of the model. The damping matrix $\underline{D}$ is computed using the same method as in the equations (4) to (6).

2.3 Actuator dynamics

In order to bring additional mechanical energy to the system, four voice coil actuators (see figure 6) are added as shown in figure 3. This technology choice is made regarding the specifications of electromagnetic actuation compared to hydraulic for instance. Voice coil actuators allow low time response and easy control of the generated force by voltage and current supply. Furthermore, the high weight of the permanent magnets is also used as passive bobweight mass which reduces significantly the mass cost of such system comparing active and passive device. During flight, the controller computes the necessary force to be generated by each actuator of the suspension. As presented in common litterature [11], the current and voltage supply of the actuators can be derived from these expressions:

$$\begin{cases} F_{act}(t) = K_f I(t) \\ U(t) \quad = L_a \dot{I}(t) + RI(t) + K_s \dot{x}_{act}(t) \end{cases} \tag{11}$$

with U, I and $x_{act}(t)$ representing respectively the voltage supply, current supply and the actuator displacement. F_{act} is the force

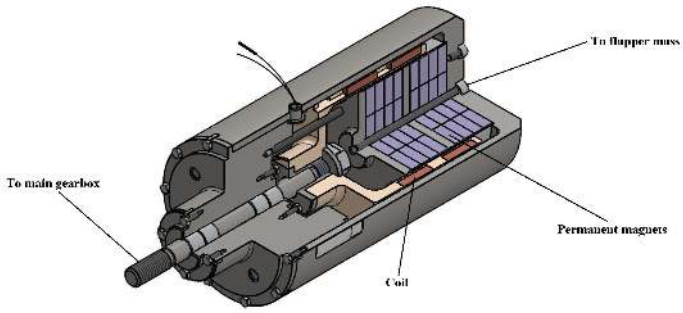

FIGURE 6: Voice coil actuator for the active SARIB® suspension

Variable	Description	Unit
K_f	force constant	$[N.A^{-1}]$
K_s	back EMF effect constant	$[V.s.m^{-1}]$
L_a	coil inductivity	$[H]$
R	coil resistance	$[\Omega]$

TABLE 3: Voice coil actuator main parameters

output generated by the actuator. All the parameters are listed in table 3.

2.4 Rotor hub input

In [1], the theoretical calculation of the dynamic rotor loads are presented. when passing from the rotating rotor fixed frame to the structure fixed frame, it is demonstrated that the forces and moments transmitted from the blades to the fuselage are in the following form:

$$\underline{\tau}_r(t) = \begin{bmatrix} \sum_{i=1}^n F_{x_i} e^{ib\Omega t - \phi_{fx_i}} \\ \sum_{i=1}^n F_{y_i} e^{ib\Omega t - \phi_{fy_i}} \\ \sum_{i=1}^n F_{z_i} e^{ib\Omega t - \phi_{fz_i}} \\ \sum_{i=1}^n M_{x_i} e^{ib\Omega t - \phi_{mx_i}} \\ \sum_{i=1}^n M_{y_i} e^{ib\Omega t - \phi_{my_i}} \\ \sum_{i=1}^n M_{z_i} e^{ib\Omega t - \phi_{mz_i}} \end{bmatrix} \tag{12}$$

The amplitude of every harmonics $ib\Omega$ is decreasing with the frequency which explains that most of the vibrational energy comes from the first component at $b\Omega$. This is tipically to reduce acceleration level in cabin around this frequency that the controller is designed for. For the Airbus Helicopter NH90, $b\Omega = 17Hz$ so the controller should emphasize on a bandwidth $b_\omega = [15-19]Hz$. Forces and moments amplitudes also change regarding to the

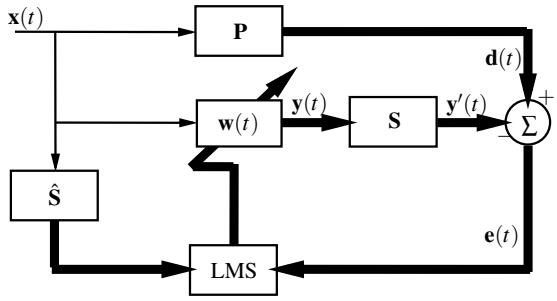

FIGURE 7: FXLMS principle method

axis, it can achieve several kN at $b\Omega$ in vertical an longitudinal axis for the helicopter considered here.

3 CONTROL PROBLEM

In a helicopter, the global objective is to improve the pilots and crew comfort. Since exposure to vibrations for humans inside transports is submitted to legislation (see [12]), some helicopters could never be certified without anti vibration devices. In order to attain such global objective, several ways of controlling the actuators of the active SARIB® can be considered:

- Take as objective function only signals from pilot seat/feet and copilot seat/feet accelerometers or a specific crew seat (local control).
- Use all accelerometers availables on the structure to set the objective function of the controller (global control).
- Use the fittings accelerometers to control the vibration transmission between the suspension and the fuselage.
- Use selected accelerometers in order to control a specific mode of the structure.
- Use force sensors on the struts to reduce the load transmisibility from main gearbox to the structure.

As long as all these objectives are not necessarily compatible and even can be opposite, a choice has to be made regarding efficiency and mission needs (crew transport for offshore is different to sea surveillance for instance).

4 CONTROLLER DESIGN: FXLMS with derivative state feedback

The controllers designed for the suspension system are called FXLMS [13] (Filtered X Least Mean Square) from the adaptive control theory also often used for noise control. This algorithm uses a reference signal (feedforward control) to generate command inputs which update at each time step to gradually reduce the RMS norm of the error signals. It is called adaptive as the controller parameters are time dependent.

The principle of FXLMS method is presented on figure 7 with P and S as the dynamic model controlled (Plant). R is defined as the number of actuators (4 for the active SARIB®) and E as the number of error sensors. The rotor RPM information is used in order to build the reference signal $x(t) = [cos(\Omega t)\ \ sin(\Omega t)]^T$. Then the reference vector $\mathbf{x}(t)$ is computed:

$$\mathbf{x}(t) = [x_1(t)\ \ x_2(t)\ \ \cdots\ \ x_L(t)]^T \tag{13}$$

L is defined as the order of the adaptative filters (length of $x(t)$). The next step consists in computong the adaptive weighting vector $\mathbf{w}(t)$:

$$\mathbf{w}(t) = [\mathbf{w}_1^T(t)\ \ \mathbf{w}_2^T(t)\ \ \cdots\ \ \mathbf{w}_R^T(t)]^T \tag{14}$$

with

$$\mathbf{w}_r(t) = [w_{r,0}(t)\ \ w_{r,1}(t)\ \ \cdots\ \ w_{r,L-1}(t)]^T, \qquad r \in [1,R] \tag{15}$$

Finally, the command vector $\mathbf{y}(t) \in \Re^{[}R \times 1]$ corresponding to the ideal signals sent to the actuators is defined as it follows:

$$\mathbf{y}(t) = [y_1(t)\ \ y_2(t)\ \ \cdots\ \ y_R(t)]^T. \tag{16}$$

Each command signal is computed by filtering the reference signal with its corresponding weighting filter $\mathbf{w}_r(t)$. This leads to the expression of the command vector $y(t)$

$$\mathbf{y}(t) = \begin{bmatrix} \mathbf{x}(t) & \mathbf{0} & \cdots & \mathbf{0} \\ \mathbf{0} & \mathbf{x}(t) & \mathbf{0} & \vdots \\ \vdots & \mathbf{0} & \ddots & \mathbf{0} \\ \mathbf{0} & \cdots & \mathbf{0} & \mathbf{x}(t) \end{bmatrix}^T \mathbf{w}(t) \tag{17}$$

$$= \mathbf{X}^T(t)\mathbf{w}(t) \tag{18}$$

$\mathbf{X} \in \Re^{[(RL)\times L]}$ is a block diagonal matrix. let $\mathbf{S}(s)$ be the transfer functions matrix between control actuators and each error sensors and $\hat{\mathbf{S}}(s)$ its estimation computed as follows:

$$\hat{\mathbf{S}}(s) = \begin{bmatrix} \hat{s}_{11}(s) & \hat{s}_{12}(s) & \cdots & \hat{s}_{1R}(s) \\ \hat{s}_{21}(s) & \hat{s}_{22}(s) & \cdots & \hat{s}_{2R}(s) \\ \vdots & \vdots & \ddots & \vdots \\ \hat{s}_{E1}(s) & \hat{s}_{E2}(s) & \cdots & \hat{s}_{ER}(s) \end{bmatrix} \tag{19}$$

The error signal vector $\mathbf{e}(t)$ measured by the E error sensors is defined as:

$$\mathbf{e}(t) = \mathbf{d}(t) - \mathbf{S}(t) * \mathbf{y}(t) \tag{20}$$

with $\mathbf{d}(t) \in \Re^{[E\times 1]}$ the unobservable disturbance vector of the system. Combining (20) with (17), the following expression can be written:

$$\mathbf{e}(t) = \mathbf{d}(t) - \mathbf{S}(t) * [\mathbf{X}^T(t)\mathbf{w}(t)] \tag{21}$$

The cost function of the algorithm is defined as the sum of the mean square errors:

$$\varepsilon(t) = \sum_{e=1}^{E} E[e_e^2(t)] \tag{22}$$

which can be approximated by

$$\hat{\varepsilon}(t) = \mathbf{e}^T(t)\mathbf{e}(n) \tag{23}$$

The adaptive weight vector is updated a each time step in the negative gradient direction to minimize the cost function $\varepsilon(t)$, this update is defined as follows:

$$\mathbf{w}(t+t_e) = \mathbf{w}(t) - \frac{\mu}{2}\nabla\hat{\varepsilon}(t) \tag{24}$$

$\mu \in \Re^{+*}$ is the arbitrary defined convergence factor of the algorithm. Depending on the system controlled, it exists a upper limit for the parameter μ to not exceed in order to avoid divergence of signal $\mathbf{y}(t)$. The gradient of (24) is expressed with respect to the r^{th} vector at each time step which leads to the following important result:

$$\nabla\hat{\varepsilon}(t) = -2[\hat{\mathbf{S}}^T(t) \circledast \mathbf{x}(t)]\mathbf{e}(t) \tag{25}$$

$$= -2\mathbf{X}'(t)\mathbf{e}(t) \tag{26}$$

Where $\circledast$ denotes the Kronecker product convolution obtained by convolving each element of $\hat{\mathbf{S}}^T(t)$ with $\mathbf{x}(t)$. The next equation presents the detailed calculation of this filtered reference matrix $\mathbf{X}'(t)$.

$$\mathbf{X}'(t) = \begin{bmatrix} \hat{s}_{11} * \mathbf{x}(t) & \cdots & \hat{s}_{E1} * \mathbf{x}(t) \\ \vdots & \ddots & \vdots \\ \hat{s}_{1R} * \mathbf{x}(t) & \cdots & \hat{s}_{ER} * \mathbf{x}(t) \end{bmatrix} \tag{27}$$

$$= \begin{bmatrix} \mathbf{x}'_{11}(t) & \cdots & \mathbf{x}'_{1E}(t) \\ \vdots & \ddots & \vdots \\ \mathbf{x}'_{R1}(t) & \cdots & \mathbf{x}'_{RE}(t) \end{bmatrix} \tag{28}$$

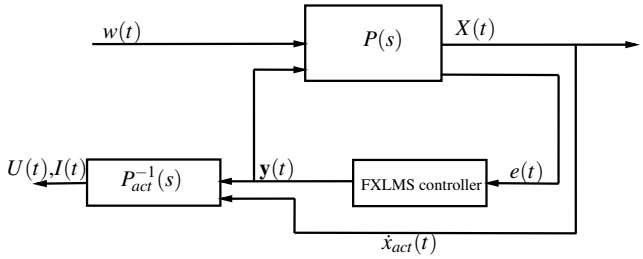

FIGURE 8: Global system representation

With $\mathbf{X}' \in \Re^{[(RL)\times E]}$. Combining the equations (24), (25) and (27), the general update equation of the weighting vector is defined as:

$$\mathbf{w}(t+t_e) = \mathbf{w}(t) + \mu\mathbf{X}'(t)\mathbf{e}(t) \tag{29}$$

In order to have a more efficient local control on some error sensors, it is possible to premultiply the matrix $\mathbf{X}'$ by a diagonal coefficient matrix $\mathbf{Q} \in \Re^{[E\times E]}$.

$$\mathbf{X}'_c(t) = \mathbf{Q}\mathbf{X}'(t) \tag{30}$$

Furthermore, it is necessary to add a leak coefficient α in the equation (29) to control the norm of the command inputs. This coefficient between 0 and 1 represents the level of attenuation wanted on the error sensors. For complex systems, crossed effects between control actuators and sensors can lead to impossible convergence to the null error on every error sensor. This phenomenon explains the need of a leak coefficient included in the equations as follows:

$$\mathbf{w}(t+t_e) = \alpha\mathbf{w}(t) + \mu\mathbf{X}'(t)\mathbf{e}(t) \tag{31}$$

On the figure 8 is represented the global system including the main plant P, the adaptive controller and the inverse dynamics P_{act}^{-1} of the actuator in order to compute the current and voltage supply necessary to generate the force signal $y(t)$.

5 SIMULATION RESULTS

The parameters shown in the table 1 and 2 are put into the model and controller equations presented before. In order to compute the transfer function estimations $\hat{s}_{er}(s)$ from each control actuator to every error sensor, the state space formulation is used. First is defined the state vector of the system $x = [q\ \dot{q}]^T$. The equations of motion can be formulated as follows:

$$\begin{bmatrix} \dot{q} \\ \ddot{q} \end{bmatrix} = \left[\begin{array}{c|c} 0 & I \\ \hline -\underline{M}^{-1}\underline{K} & -\underline{M}^{-1}\underline{D} \end{array}\right] \begin{bmatrix} q \\ \dot{q} \end{bmatrix} + \left[\begin{array}{c|c} 0 & 0 \\ \hline \underline{S} & \underline{S_c} \end{array}\right] \begin{bmatrix} \underline{\tau} \\ \underline{u_c} \end{bmatrix} \tag{32}$$

with $\underline{S_c} \in \Re^{[2(p+n)\times E]}$ the direction control matrix and $u_c \in \Re^{[E\times 1]}$ the command vector containing all command inputs. This formulation leads to the state space representation

$$\begin{cases} \dot{x}(t) = Ax(t) + Bu(t) \\ \dot{y}(t) = C\dot{x}(t) + Du(t) \end{cases} \tag{33}$$

One can notices that the observation matrix C is multiplying the time derivative of the state vector. This method, different than the classical one using the state vector allows to directly control the acceleration measure signals.

$$\hat{S}(s) = Cs(sI - A)^{-1}B_c + D_c \tag{34}$$

With the matrices B_c and D_c representing the columns of B and D from (33) multiplied by the control inputs (see $\underline{S_c}$ from (32)). Now that the frequency response of each sensor to every control input is estimated, the system can be simulated. The rotor input force used to compare the performance of the controllers is a variable frequency sine wave of 8kN arbitrary amplitude in vertical direction varying from 15Hz to 19Hz in a 10s time simulation.

All the equations presented in the section before are used to design the adaptive FXLMS controller. As a comparison criteria, the RMS value of acceleration level on each sensor of the fuselage is taken. Three different controllers are computed changing one from another in the error sensors selected:

- Controller 1: 2 nodes in the cockpit corresponding to the pilot and copilot seat.
- Controller 2: 2 nodes in the cabin corresponding to the frame number 6 situated under the main gearbox (high vibration level).
- Controller 3: 4 nodes corresponding to the fittings linking the suspension to the structure in order to stop vibrations propagation closer to the source.
- Controller 4: 2 nodes in the nose of the structure to control a bending mode situated around 17Hz.

On the tables 4, 5 and 6 are presented the main results of the simulations performed for each controller. The figure 9 presents level maps of RMS acceleration value in the structure. On these maps the x axis represents the fuselage width and the y axis its length ($y = 0$ means the helicopter front part). All these calculations are done with a leak coefficient $\alpha = 1 - 10^{-6}$ and a convergence factor $\mu = 3.10^3$. An exception has been made for the controller 4 with $\mu = 5.10^2$ due to the structural bending mode controlled generating fast phase changes on the error sensors signal placed in the nose of the fuselage.

Simulation results show that a 20% reduction in RMS acceleration level can be achieved with the controller 3. The controller 1, emphasizing on the control of the cockpit amplifies the vibration level in the cabin (+7%). However the reverse behaviour is not verified since the controller 2 minimizes the vibration of the frame 6 in the cabin. This phenomenon can be explained by the location of the main gearbox on the frame 6 of the structure. Indeed, these nodes are closer to the vibration source and allow better control of their propagation. Following this logic, it also explains the excellent results obtained whith the controller 3 due to the very close position in the fuselage of the error sensors from the vibration source: the rotor hub. The controller 4 obtains good results minimizing the bending mode effect on the cockpit (-22.49%) but deteriotates the comfort in the cabin.

One can notices in the table 5 the low power and force needed to control the vibrations of the structure around 17Hz due to the passive DAVI suspension SARIB®. Comparing the

	cockpit	cabin	global
controller 1	-11.2%	+7.21%	+1.06%
controller 2	-24.51%	-12.1%	-16.24%
controller 3	-42.13%	-8.26%	-19.55%
controller 4	-22.49%	+4.69%	-4.37%

TABLE 4: results from the simulation: 8kN vertical force input on the rotor hub from 15Hz to 19Hz in 10s, average vibration reduction compared to passive SARIB® suspension on different part of the helicopter for each controller.

	maximum force norm [N]				command power [W]			
	FR	FL	RR	RL	FR	FL	RR	RL
controller 1	78.7	80.65	41.83	29.69	5.8	6.1	1.59	0.73
controller 2	92.6	89.5	32.2	34.7	8.05	7.47	0.88	0.97
controller 3	176	161	42	40	28.86	24.2	2.37	2.08
controller 4	81	80	38	39	6.32	6.05	1.32	1.44

TABLE 5: results from the simulation: power consumption and actuator force necessary to each controller(FR: front right, FL: front left, RR: rear right, RL: rear left).

	voltage supply [V]				current supply [A]			
	FR	FL	RR	RL	FR	FL	RR	RL
controller 1	4.28	3.11	1.51	1.21	2.02	2.07	1.08	0.66
controller 2	3.5	3.36	1.06	1.15	2.38	2.3	0.83	0.9
controller 3	8.17	7.52	2.35	2.37	4.54	4.66	1.09	1.04
controller 4	3.77	3.11	1.37	1.25	2.06	0.99	0.99	1

TABLE 6: results from the simulation: voltage and current supply for the actuators (FR: front right, FL: front left, RR: rear right, RL: rear left).

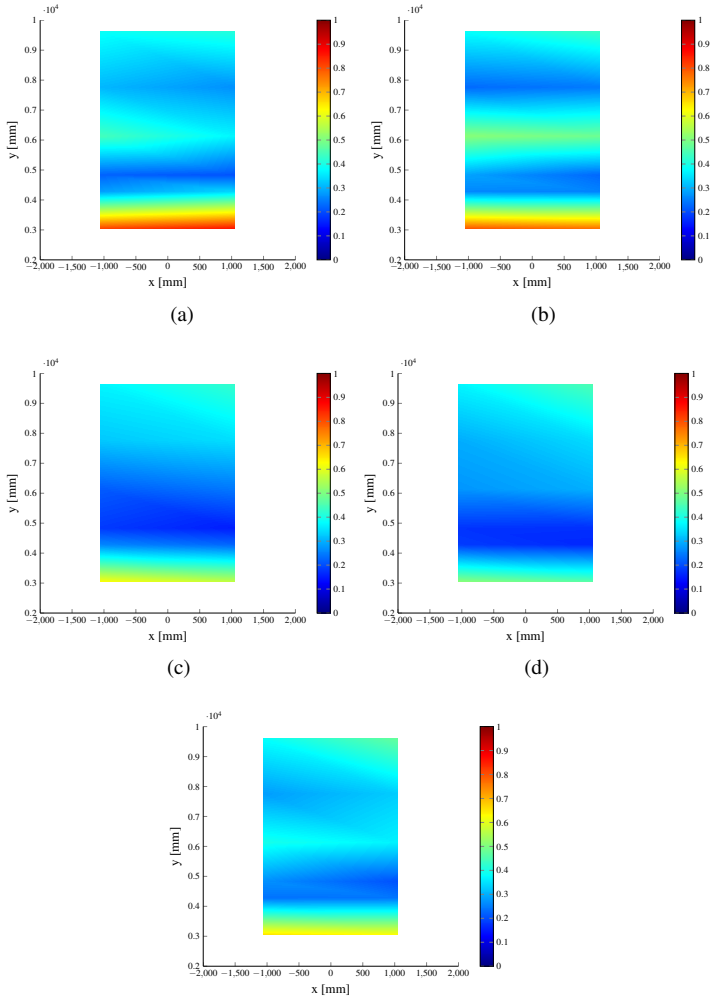

FIGURE 9: RMS acceleration level maps for each controller: passive suspension (a), controller 1 (b), controller 2 (c), controller 3 (d), controller 4 (e).

four controllers, the number 2 appears to be best compromise between efficiency and power consumption while the number 3 is the most efficient. These results show that local control or global control of vibration level in the structure always brings compromise in terms of performance localization. However, this problem is canceled when the error sensors are placed directly in the main vibration propagation path as for the controller 3.

An other simulation is performed at a fixed frequency of 17Hz with the objective to observe the convergence of the weighting filters $\mathbf{w}(t)$. The results are presented on figure 10. The controller is switched on at t=4s and the convergence is achieved in about 4 seconds. Even if the system is excited at the nominal frequency of the passive DAVI suspension, a reduc-

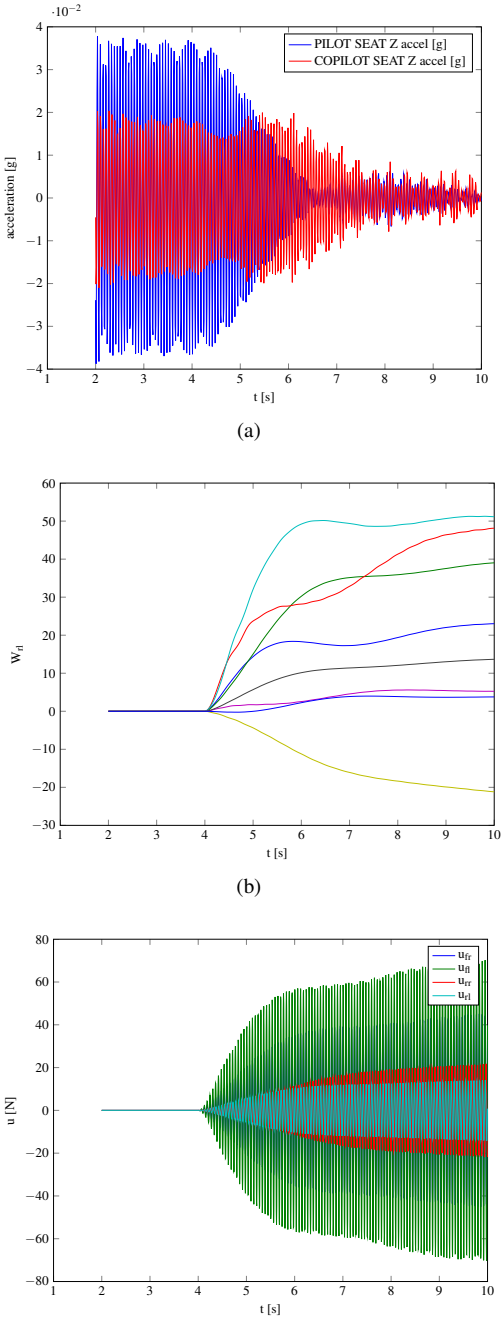

FIGURE 10: switch off/on of the FXLMS control at t=4s at 17Hz (controller 1), 8kN vertical force input on the rotor hub: acceleration level on the error sensors (a), weighting filter values (b), command forces (c).

tion of 21.2dB on the pilot seat and 9.36dB on the copilot seat is still reached. Even if the suspension system is symmetrically designed, a clear dissimmetry of control force from the actuators appears. This behaviour can be observed and anticipated by the use of a realistic modal base as structure to isolate instead of a rigid body. It can be noticed that front actuators needs to develop aproximately two times the forces needed for rear actuators. Furthermore, the high number of estimated transfer functions necessary to run the FXLMS algorithm ($E \times R$) and the high importance of crossed effects between actuators and error sensors due to their non-colocalization increase the time for convergence of the weighting factors and so decrease the controller global efficiency in time response and acceleration level reduction. However, this conclusion supports the idea from previous part that controlling the vibrations transmission directly with error sensors between the suspension system and the structure improves the algorithm efficiency by minimizing phase delay and crossed effects from actuators to sensors.

6 CONCLUSION

A complete multibody model of a passive helicopter suspension was developed and coupled to a fuselage modal base. Then an adaptive FXLMS controller with acceleration error sensors on the helicopter structure was set up in order to command a hybrid suspension (passive vibration absorbers coupled to force actuators) based on DAVI principle. Four controllers have been tested to compare different locations for the error sensors: in the nose, the cockpit, the cabin and under the fittings of the suspension. Results show that with command forces lower than 180N we proven to decrease the RMS vibration level in the whole structure by 20%. Furthermore, for command actuators placed between the source and the structure to control, minimizing the vibration level directly on the vibration main propagation path is much more efficient than controlling local sensors inside the structure. This conclusion allows to consider relevant the choice of such active anti-vibration device regarding classical cabin vibration absorbers with only local effects in terms of global performance and hardware integration.

REFERENCES

[1] A.R.S. Bramwell, George Bone, D. B., 2001. *Bramwells Helicopter Dynamics, second edition*. Butterworth Heinemann.

[2] Flannelly, W., 1976. "The dynamic anti-resonant vibration isolator". *AHS*.

[3] Michael R. Smith, BELL Helicopters W. Scott Redinger, L. C., 1999. "The model 427 pylon isolation system". *AHS*.

[4] T.J. SUTTON, S. E., and JESSOP, M. B. K. H. D., 1997. "Active isolation of multiple structural waves on a helicopter gearbox support strut". *Journal of Sound and Vibration,* ***205***, pp. 81–101.

[5] Berengere Vignal, Tomasz Krysinski, E., 2005. "Development and qualification of active vbration control system for the eurocopter ec225/ec725". *AHS*.

[6] Benjamin Kerdreux, J. J. E., 2012. "Vibration comfort through active cabin vibration control and its certification on ec130t2". *ERF*.

[7] McGuire, D. P., 2006. "Active vibration control using fluidlastic pylon strut". *AHS*.

[8] de Wouw, N. V., 2010. *Multibody Dynamics Lecture Notes*. Technische Universiteit Eindhoven.

[9] P.Cranga, 2005. "Helicopter dynamic behavior contribution to general architecture definition". PhD thesis, Ecole doctorale Mecanique, Energetique, Genie civil, Acoustique (MEGA).

[10] Craig Jr. R.R., Bampton, M., 1968. "Coupling of substructures for dynamic analysis". *AIAA,* ***6***, pp. 1313–1319.

[11] Preumont, A. *Vibration Control of active structures, an introduction, 3rd edition*. Springer.

[12] ISO-2631, 1978. "Guide for the evaluation of human exposure to whole-body vibration".

[13] Sen M.Kuo, D. R., 1996. *Active Noise Control Systems, Algorithms and DSP implementations*.